ELSEVIER

Materials Science and Engineering A349 (2003) 298–305

MATERIALS SCIENCE & ENGINEERING A

www.elsevier.com/locate/msea

Correlations between operating conditions, microstructure and mechanical properties of twin wire arc sprayed steel coatings

G. Jandin [a], H. Liao [a,*], Z.Q. Feng [b], C. Coddet [a]

[a] *LERMPS, Université de Technologie de Belfort-Montbéliard, 90010 Belfort Cedex, France*
[b] *IUP/CEMIF, Université d'Evry Val d'Essonne, 91020 Evry Cedex, France*

Received 22 April 2002; received in revised form 8 October 2002

Abstract

An experimental design matrix was set up in which carbon steel coatings were deposited with a twin wire arc spray gun (TAFA 9000™), using either compressed air or nitrogen as spraying gas. The coating's mechanical properties were studied. Some correlations were made between these properties, spraying conditions and the microstructure of the deposits. Young's modulus was estimated by the single beam method using finite element modeling. Results show that direct relationships do exist between spray conditions, oxide content in the coating and microhardness. Young's modulus of the coatings depends on the lamella thickness and the oxide content. When increasing the compressed air flow rate, Young's modulus increases at first because smaller particles and finer lamellae were made and it decreases later because of a higher oxide content. The increase of nitrogen flow rate lowers the oxide content and increases Young's modulus.

Keywords: Twin-wire arc spraying; Microstructure; Single beam method; Young's modulus

1. Introduction

Twin wire arc spraying is known to be one of the less expensive ways of thermal spraying [1]. The material to be deposited is introduced into the system in the form of two wires serving as consumable arc electrodes. One of the traditional applications is to produce protecting coatings for infrastructures. Moreover, the technological development of wire arc spray systems opens other ranges of applications, such as mould spray forming [2,3]. The arc process has generally higher spray rates than other spray processes reaching easily 15 kg h^{-1}. This range of spray rate mostly depends on the nature of the sprayed material and wire diameter. Thick coatings can be built up rapidly and economically [1].

Materials that can be sprayed are metallic wire (iron, copper, zinc) or cored wire containing powders (for example WC/Co) in order to produce composite materials.

Compressed air is commonly used in the wire arc process because of its low cost and availability. However the oxide content of such sprayed coatings is relatively high due to the oxidation of molten droplets. Thus interlamellar bond strength and machinability of coatings are reduced due to their oxide content. The use of air leads also to a burn off of the carbon when spraying steels, which is of course detrimental to the coatings characteristics. As a countermeasure, nitrogen can be proposed as atomizing gas in order to decrease oxide rate and carbon depletion of steel coatings [4].

Experimental design approaches have already been investigated, by Varacalle and Saravanan [5,6] for example, for a better understanding of the influence of spray parameters on coating microstructure. However, only a few studies have been undertaken to analyze correlations between spray parameters, microstructure aspects and mechanical properties of coatings. In this study, two ways of characterization have been followed.

* Corresponding author. Tel.: +33-3-84-58-32-42; fax: +33-3-84-58-32-86
E-mail address: hanlin.liao@utbm.fr (H. Liao).

0921-5093/02/$ - see front matter
PII: S0921-5093(02)00767-0

Table 1
Summary of experimental design matrix and results using compressed air as atomized gas

Exp. No.	Power, W	Primary spray pressure, Bar (psi)	Secondary spray pressure, Bar (psi)	Total gas flow rate, N m^3 h^{-1}	Oxide content, %	Young, GPa	Hardness, HV300
01	1000	2.8 (40)	1.0 (15)	93	29	63.5	305.7
02	1000	2.8 (40)	2.4 (35)	107	29.5	115.8	344.7
03	1000	2.8 (40)	3.8 (55)	110	31	138.5	353.8
04	1000	2.8 (40)	5.2 (75)	122	32	144.4	321.9
05	1000	4.9 (70)	1.0 (15)	100	28	105.3	354.7
06	1000	4.9 (70)	2.4 (35)	116	32	107	300.0
07	1000	4.9 (70)	3.8 (55)	134	34.5	126.3	369.9
08	1000	4.9 (70)	5.2 (75)	144	28.5	53.8	321.8
09	2200	2.8 (40)	1.0 (15)	93	22	98.8	278.8
10	2200	2.8 (40)	2.4 (35)	107	20	64.3	291.5
11	2200	2.8 (40)	3.8 (55)	110	21	104.6	292.7
12	2200	2.8 (40)	5.2 (75)	122	22	91.7	313.1
13	2200	4.9 (70)	1.0 (15)	100	23.5	137.4	296.1
14	2200	4.9 (70)	2.4 (35)	116	21.5	150	281
15	2200	4.9 (70)	3.8 (55)	134	23.5	105.1	322
16	2200	4.9 (70)	5.2 (75)	144	22.5	110.6	337.3
17	3100	2.8 (40)	1.0 (15)	93	18	89	304.5
18	3100	2.8 (40)	2.4 (35)	107	19	102.9	297.9
19	3100	2.8 (40)	3.8 (55)	110	21	96.5	287.2
20	3100	2.8 (40)	5.2 (75)	122	21.5	100.9	324.8
21	3100	4.9 (70)	1.0 (15)	100	22	84.4	276.3
22	3100	4.9 (70)	2.4 (35)	116	21	105.2	299.2
23	3100	4.9 (70)	3.8 (55)	134	22	101.9	328.4
24	3100	4.9 (70)	5.2 (75)	144	22.5	91.3	366.9
25	4000	2.8 (40)	1.0 (15)	93	18	79	281.6
26	4000	2.8 (40)	2.4 (35)	107	15.5	127.7	306.3
27	4000	2.8 (40)	3.8 (55)	110	16	101.9	275
28	4000	2.8 (40)	5.2 (75)	122	18	86.4	302.8
29	4000	4.9 (70)	1.0 (15)	100	21	95.2	270.4
30	4000	4.9 (70)	2.4 (35)	116	20	90.6	282.8
31	4000	4.9 (70)	3.8 (55)	134	21.5	83.8	304.3
32	4000	4.9 (70)	5.2 (75)	144	26.5	79.5	332.9

Table 2
Summary of experimental design matrix and results using nitrogen as atomized gas

Exp. No.	Power, W	Primary spray pressure, Bar (psi)	Secondary spray pressure, Bar (psi)	Total gas flow rate, N m^3 h^{-1}	Oxide content, %	Young, GPa	Hardness, Hv300
N2-01	3100	2.8 (40)	1.0 (15)	93	16.5	120.6	376.7
N2-02	3100	2.8 (40)	2.4 (35)	107	13.6	114.5	363.9
N2-03	3100	2.8 (40)	3.8 (55)	110	15.1	104.5	321.6
N2-04	3100	2.8 (40)	5.2 (75)	122	13	110.6	320.7
N2-05	3100	4.9 (70)	1.0 (15)	100	15.7	116.8	325.8
N2-06	3100	4.9 (70)	2.4 (35)	116	13.6	120.6	318.1
N2-07	3100	4.9 (70)	3.8 (55)	134	12.6	136.0	348.4
N2-08	3100	4.9 (70)	5.2 (75)	144	12.5	144.7	342.5

Firstly, a full experimental design matrix has been conducted for determining relationships between spray conditions (power supply and gas pressures) and microstructure, microhardness and Young's modulus of coatings, using compressed air as atomizing gas. Secondly, using identical spray parameters, a comparison was made between the use of air and that of nitrogen.

2. Experiment

2.1. Twin wire arc spraying

In this process, two consumable wires are fed automatically to meet at a point in an atomizing gas stream. An electrical potential difference (18–40 V), with a current of 35–350 A, is applied across the wire electrodes and melts the tips of both wires. The atomizing gas is directed across the arc zone, shearing the molten part of the wires to form the atomized spray [7]. In this study a wire arc spray gun TAFA 9000™ with a converging nozzle was used. There are two air inputs in this equipment; a primary gas for normal use and a secondary gas that flows through the same nozzle for increasing the total gas flow and allowing a better constriction of the spray stream. This is known to influence the coating quality through higher particle velocities and higher local pressure of spray gas [8,9]. On the TAFA arc spray system, electric voltage and current can be adjusted independently. The value of the current is automatically connected to wire feed rate; e.g. when the current increases, the wire feed rate will increase simultaneously.

2.2. Coating deposition

The wire arc spray gun was fixed onto a 6-axis ABB IRB4400™ robot to ensure repeatable kinetic motion. Carbon (0.80C) steel wires (TAFA 38T®) with a diameter of 1.6 mm were used as sprayed material. Coatings were built onto 316L, $80 \times 20 \times 1.5$ mm^3 steel plates. Specimens were fixed on a 380 mm diameter drum, rotating with a speed of 60 turns min^{-1}. The traverse speed was 10 mm s^{-1} while the stand-off distance was 200 mm.

The experimental design matrix when using compressed air as atomizing gas (Table 1), was established with three variable spray parameters: the arc power, the primary atomizing gas pressure and the secondary atomizing gas pressure. In this work the voltage was fixed to 30 ± 1 V. Therefore, a characteristic value of four levels was chosen as the electric power: 1000, 2200, 3100 and 4000 W.

The primary gas, which enables the separation of the molten part from the wires and carries the molten particles until impacting the substrate, was used with 4

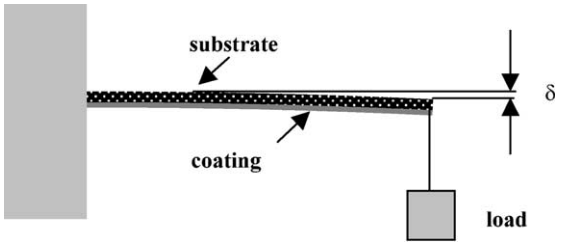

Fig. 1. Schematic description of the system for measuring Young's modulus of coating.

values in pressure: 1.0, 2.4, 3.8 and 5.2 bars. The Arc-Jet® secondary gas was used for increasing the speed of the spray stream and its constriction at two levels (2.8 and 4.8 bars). In fact, because the two gases meet together before entering the nozzle in the spray gun and for a better understanding of the phenomena, the total gas flow rate was measured and considered as the significant parameter.

When nitrogen was used as spraying gas, a single value of the electrical power (3100 W) was considered, whereas primary and secondary spray pressure varied as described before. The corresponding experimental design is presented in Table 2. All results of oxide content, Young's modulus and microhardness are also presented in the same table.

2.3. Coating characterization

Young's modulus was evaluated using a single point cantilever beam method from the measurement of the deformation of coated 316L steel plate while a bending moment is applied (Fig. 1). Coatings were submitted to a compressive stress. A computer program based on the ANSYS™ finite element software was used to determine Young's modulus Ec of the coating from the measured

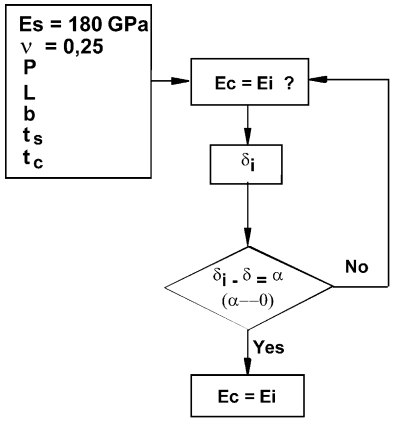

Fig. 2. Schematic description of the algorithm used for FEM resolution. where: s and c represent the substrate and the coating, respectively, subtitle i represents iterative values of calculations. E and ν, are the Young's modulus and Poisson's ratio of the material. L, b, t represent the dimension of the specimen (length, width and thickness), P and δ are the applied load and the related deformation.

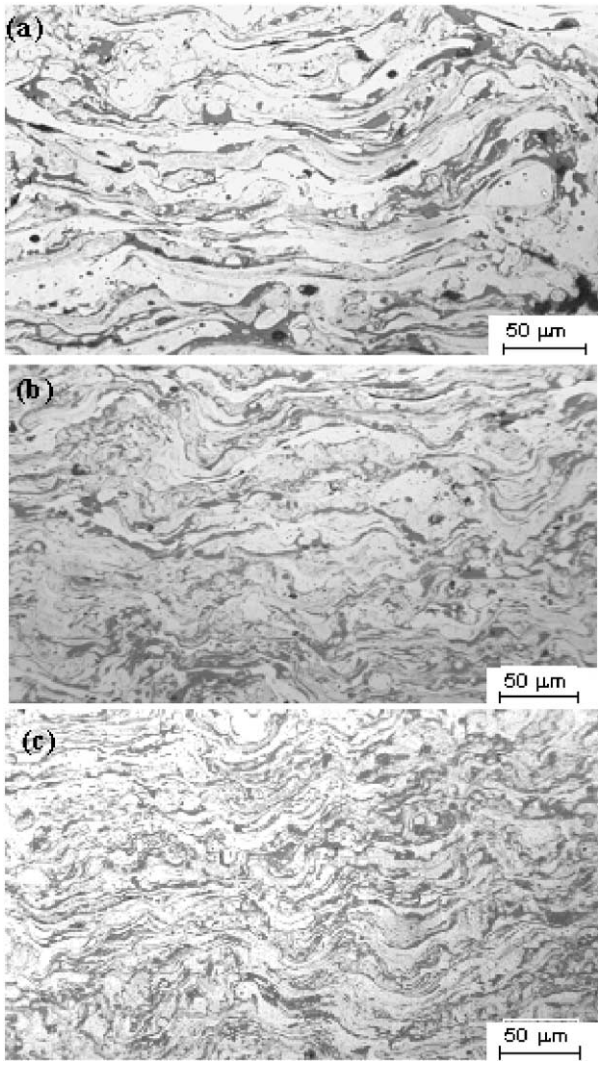

Fig. 3. Cross-sections of steel coatings with air atomization; (a) low flow rate (94 N m^3 h^{-1}), sp. 17; (b) medium flow rate (110 N m^3 h^{-1}), sp. 19; (c) high flow rate (144 N m^3 h^{-1}), sp. 24.

deformation δ of the plate (Fig. 2). An initial value of the coating Young's modulus is entered in the program. If the calculated deformation is the same as that determined experimentally, then the value of Young's modulus is found, otherwise a new value must be tested. Of course, several parameters have to be defined before calculation: thickness of the coating (t_{ic}) and that of the substrate (i_{ts}), the length and the width of the plate (L, b), Young's modulus and Poisson's ratio of the substrate ($E_s = 180$ GPa, $\nu_s = 0.25$) Poisson's ratio of the coating, which is also required for the calculation was estimated to be $\nu_c = 0.20$. Details of this method and error analysis will be described elsewhere [10]. Optical micrographs showing coating morphology were obtained from polished coating cross-sections, using reflected light microscopy with a green filter for improved contrast at 250× magnification. Image analysis was used to determine porosity and oxide content from the

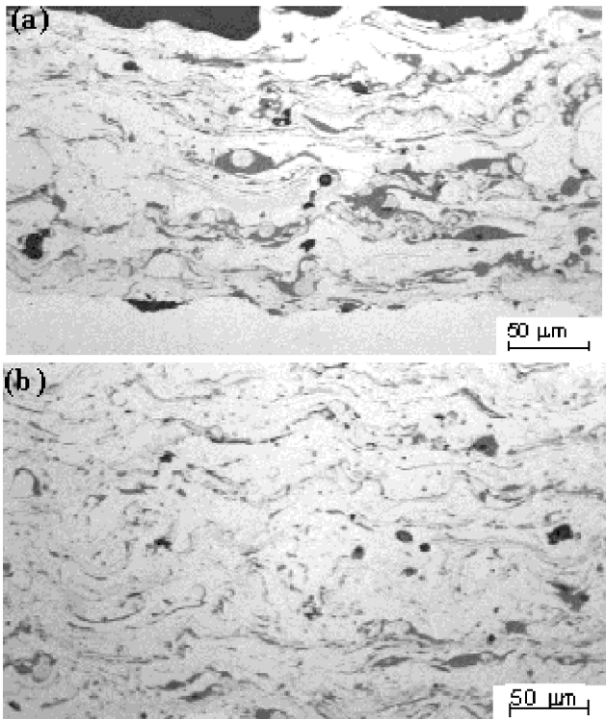

Fig. 4. Cross-sections of steel coatings with nitrogen atomization (a) nitrogen atomization, low flow rate (94 N m^3 h^{-1}), sp. N2-01; (b) high flow rate (144 N m^3 h^{-1}), sp. N2-08.

polished coating cross-sections. The analysis of gray levels enables to distinguish the different features of coating microstructure (GRAFTED™ software). Average results were obtained by measuring porosity and oxide proportion at three random locations for each sample. Vickers microhardness measurements were carried out on coating cross-sections using a load of 300 g for 15 s. Ten measurements were made at random locations on each sample. Glow discharge spectrometry (GDS) was used to determine the amount of carbon and oxygen in the deposits.

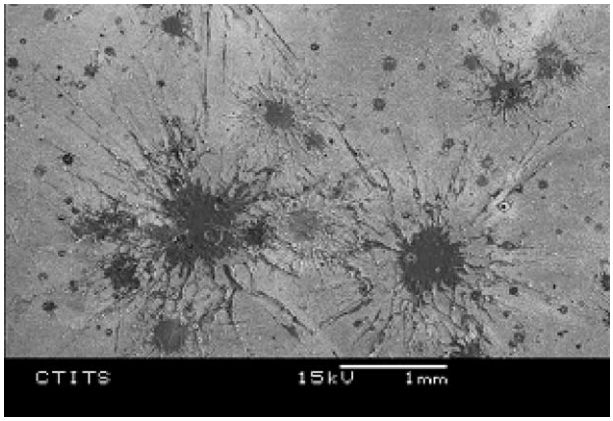

Fig. 5. Impact of sprayed particles onto polished steel substrate using low spray pressure in air atomization, average diameter: 760 µm (power 3100 W, air flow rate: 94 N m^3 h^{-1}).

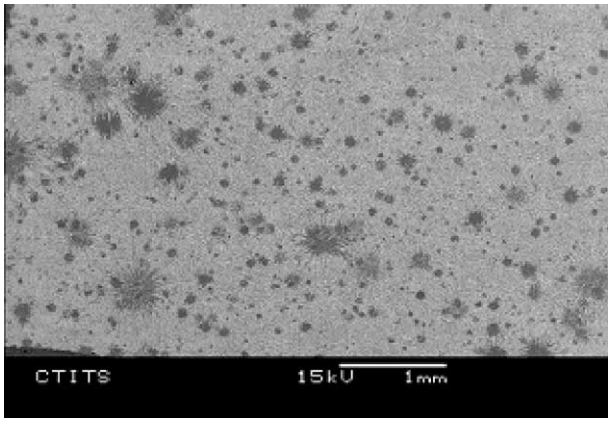

Fig. 6. Impact of sprayed particles onto polished steel substrate using high spray pressure air atomization, average diameter: 122 µm (power 3100 W, air flow rate: 144 N m^3 h^{-1}).

3. Results and discussion

3.1. Microstructures

As shown in Fig. 3, porosity levels remain rather low for all coatings, with values ranging from 1 to 2%, as estimated by image analysis. Furthermore, the main part of this porosity is believed to be due to the removal of brittle oxides while polishing the specimen. Then the influence of spraying parameters on the coating porosity appears rather small in the studied range.

Cross-section micrographs of coatings built with the power 3100 W are presented in Figs. 3 and 4. It can be seen that very thick lamellae, more than 10 µm, are produced with low gas flow rate (94 N m^3 h^{-1}, Fig. 3a

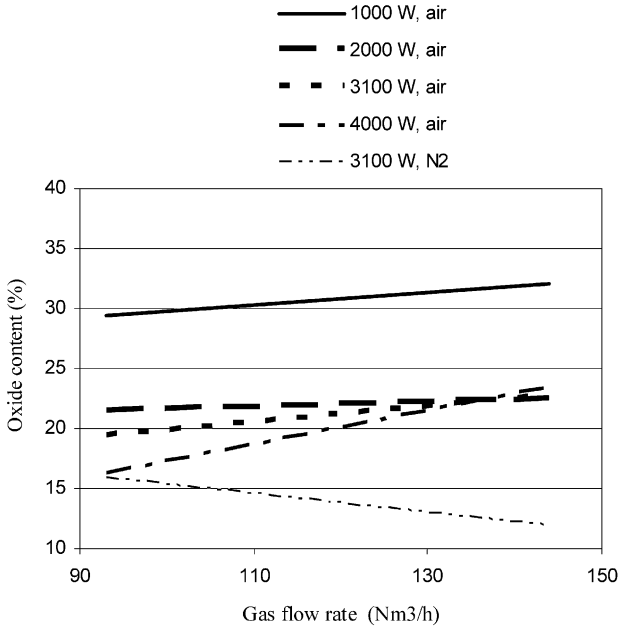

Fig. 7. Oxide content as a function of total gas flow rate with various power levels.

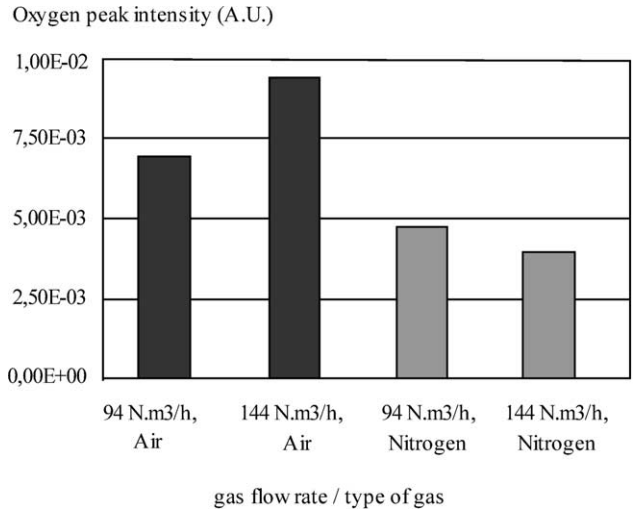

Fig. 8. Qualitative comparison of oxygen content in coatings (power: 3100 W).

and Fig. 4a) whereas thin lamellae, thinner than 5 μm, are generated while spraying with a high gas flow rate (144 N m^3 h^{-1}, Fig. 3c and Fig. 4b). The gas flow rates then have a major influence on the thickness of lamellae. The higher the gas flow rate, the thinner the lamellae. In this latter case, a quicker shearing of molten particles from solid wire occurs, leading to smaller droplets [11–13]. It is also verified in this way that it is the total gas flow rate which is the crucial parameter rather than the primary or secondary gas pressures.

SEM micrographs of particle impacts onto steel substrates at different gas flow rate values are shown in Figs. 5 and 6. It is also observed from these figures that when the atomizing gas flow rate is low, very large

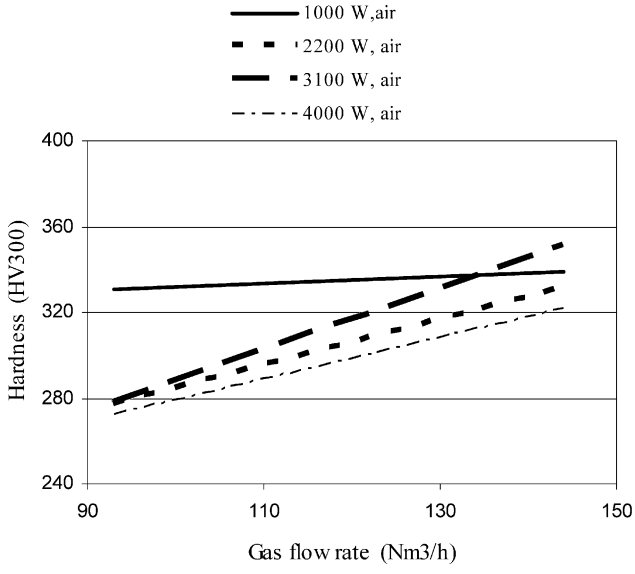

Fig. 9. Evolution of deposits hardness versus total gas flow rate, testing various power levels, spraying gas: compressed air.

splats are formed, their contribution to the build-up of the coating is then greater than that of smaller particles.

The influence of spray gas flow rate on coating oxide content is shown in Fig. 7. While an increase of gas flow causes an increase in oxide content when spraying with air, the opposite phenomenon occurs with the use of nitrogen. Image analysis results are validated with GDS evaluation of oxygen content as shown in Fig. 8, with a total flow rate that is either the lowest (94 N m^3 h^{-1}) or the highest (144 N m^3 h^{-1}). Speculation on the fact that smaller droplet size increases the contact surface area with oxygen so leading to higher oxidation rates is available: the higher the gas flow, the higher the oxide content. On the contrary, when nitrogen is employed as spray gas, oxide content is drastically lower: this inert gas protects iron from oxygen, keeping low oxygen partial pressure near molten particles and preventing their oxidation.

One thousand Watt is not a commonly used parameter (only about 33.3 A current). With this weak current and low wire feed rate, droplets formed at the wire tip seem to stay there for a long time, which increases the oxidation time. Hence, bigger lamellae and a high oxide content were observed in the coating sprayed with a power of 1000 W.

For other coatings, while the influence of gas flow rate on the oxide content is relatively high, that of power level remains rather small; meanwhile an increase of current intensity generally leads to a decrease in the coating oxide content (Fig. 7). Since wire feed rate increases automatically with current intensity, it can be assumed that in the case of higher power for a same air flow rate, there is less exchange between air and material, and therefore particles are less heated and oxidized. Moreover, the mean particle size becomes also larger when increasing the material feed rate according to the measurement of collected particles [14].

3.2. *Dependence of microstructure and microhardness on spray parameters*

Fig. 9 presents the coating hardness as a function of the atomizing gas flow rate for different power levels. For ‘standard’ conditions (2200, 3100 and 4000 W), hardness reaches almost identical values for fixed gas flow rates, whereas ‘non-standard’ parameters (1000 W) lead to a higher hardness. Since the trends for hardness and oxide content are similar and as it is generally assumed that hardness can be correlated to oxide content of coatings [6], it is not surprising to find a relationship between coatings oxide content and hardness (Fig. 10) for both spray conditions (nitrogen and air). Presented results also show that, when compressed air is the atomizing gas, the general trend is an increase of hardness with oxide content. For example, for 14 specimens having an average oxide content of $20 \pm 1.5\%$,

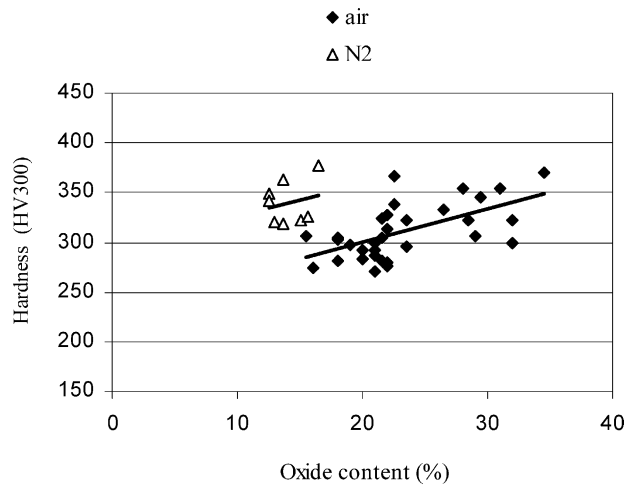

Fig. 10. Cross-section hardness (HV_{300}) versus oxide content, using either nitrogen or air as spraying gas.

the average hardness is 295 ± 8 HV_{300}, whereas for 8 specimens having an oxide content of $30 \pm 2\%$ hardness reaches 334 ± 12 HV_{300}. The use of nitrogen modifies both oxidation rate and hardness, but the trends are the same. Moreover, a lower decarburization rate due to nitrogen (Fig. 11) could explain the difference between coatings deposited using nitrogen as spraying gas which have a residual carbon content near 0.5 against 0.2% for a coating sprayed with air. The amount of carbon governs the microstructure and coating hardness.

3.3. Young's modulus

Young's moduli of coatings identified by the cantilever beam method are listed in Tables 1 and 2 for the two atomizing gases. When compressed air is used as spraying gas, average Young's modulus is close to $100 \pm$ 10 GPa, whereas use of nitrogen permits an average value of 120 ± 10 GPa.

Fig. 12 shows a simplified evolution of both the Young's modulus of coatings and the oxide content as a function of the gas flow rate for nitrogen conditions while Fig. 13 presents the evolution of Young's modulus of coatings, for various power spray parameters (the values for 2000 W are not presented because the results scatter). It can be seen in Fig. 12 that the Young's modulus of coatings built using nitrogen as spraying gas increases with the gas flow rate whereas the oxide content decreases, both in a rather linear way. On the contrary, in the case of air (Fig. 13), a non-linear trend can be observed; first, Young's modulus increases with air flow rate to a maximum value (120 N m^3 h^{-1}) and then it decreases again. This phenomenon probably

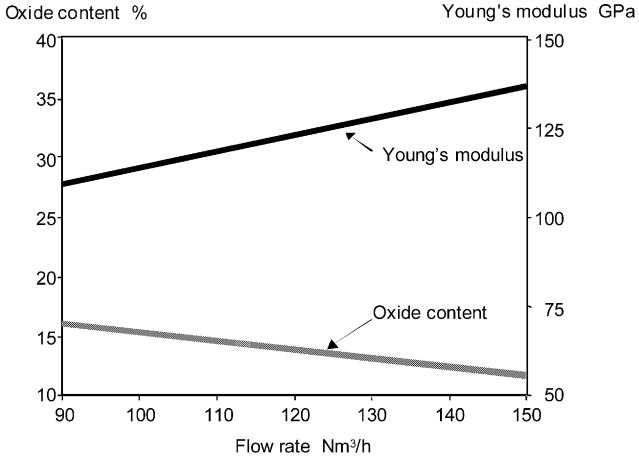

Fig. 12. Young's modulus versus nitrogen flow rate and oxide content.

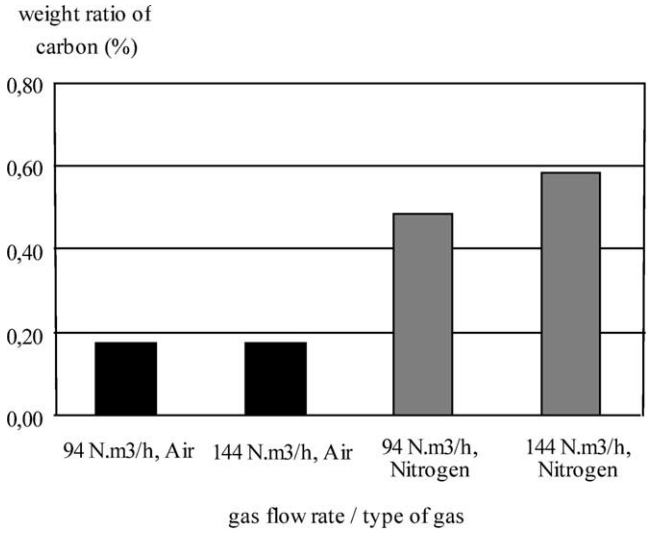

Fig. 11. GDS measurements of weight ratio of residual carbon in coatings (power supply: 3100 W).

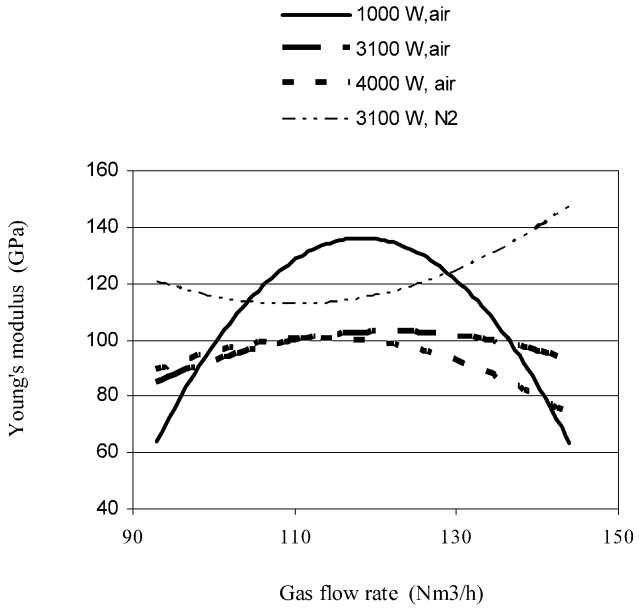

Fig. 13. Young's modulus versus gas flow rate.

results from two opposite mechanisms. On the one hand, the higher the particle flattening degree and the more homogeneous the microstructure, the higher is the modulus; for twin wire arc spray, an increase of the gas flow rate leads to an increase in the degree of flattening of droplets (Fig. 6), leading then to an increase in the homogeneity of the coating (Fig. 3c). On the other hand, for metallic sprayed coatings and because of low interlamellar bonding, oxides are considered as defects in the coating: the higher the oxide content, the lower the modulus. It was observed that an increase in air flow rate leads to an increase in oxide content (Figs. 7 and 8). Therefore, an increase in the air flow rate could be detrimental to Young's modulus of coatings. These two assumptions are considered as constituting the basic mechanism explaining the dependence of Young's modulus of sprayed steel on the air flow rate. In the case of nitrogen the oxygen content is much lower and the modulus continues to increase with the flow rate due to the corresponding increase in homogeneity of the coating.

4. Conclusion

Mechanical properties of steel coatings built with a twin wire arc spray system were investigated. The use of an experimental design enabled us to determine relationships between spray parameters, microstructure and corresponding hardness and Young's modulus of the coatings.

(1) Oxide content of course appears mainly related to the type of gas used as atomizing gas: nitrogen lowered oxide content compared to air, but the atomizing gas spray flow rate has also a main influence on the oxide content: the higher the nitrogen flow rate or the lower the air spray flow rate, the lower the oxide content.

(2) The type of spray gas influences the hardness of coatings. For both spray conditions, a higher oxide content leads to a higher hardness, but when using nitrogen, a better carbon retention allows an increase in hardness for a given oxide content.

(3) Young's modulus of coatings was identified through a single point cantilever beam measurement combined with a finite element calculation. Splat thickness and oxide content, which depend on the spraying conditions, notably influence the modulus. Again, larger values are obtained with nitrogen but careful selection of spray parameters may allow similar results when spraying with air.

Acknowledgements

The authors especially express their thanks Dr V. Monin for his help in designing the cantilever beam apparatus. They also gratefully acknowledge the assistance of Dr M. Verdier and Dr J.-F. Laithier for their valuable input in helping us to conduct this evaluation.

References

[1] M.L. Thorpe, Adv. Mater. Processes 143 (1993) 50.
[2] P.S. Fussell, Ph.D. Thesis, Carnegie Mellon University, PA, USA, 1994.
[3] G. Jandin, H. Liao, C. Coddet, Chinese Surface Engineering Society, in: B. Xu, (Ed.), Proceedings of International Conference on Advanced Manufacturing Technology, Xi'an, China, 1999, p. 102.
[4] X. Wang, D. Zhuang, E. Pfender, J. Heberlein, W. Gerberich, High Temperature Society of Japan, in: A. Ohmori, (Ed.), Proceedings of the Fifth International Thermal Spray Conference, Osaka, Japan, 1995, p. 1209.
[5] D.J. Varacalle Jr., G.C. Wilson, L.B. Lundberg, D.L. Hale, V. Zanchuck, W. Kratochvil, G. Irons. in: C.C. Berndt, S. Sampath, (Eds.), Proceedings of the Eighth National Thermal Spray Conference, Houston, USA. ASM International, Materials Park, OH, USA, 1995, p. 373.
[6] P. Saravanan, V. Selvarajan, S.V. Joshi, G Sundarajan, J. Phys. D: Appl. Phys. 34 (2001) 131.
[7] X. Wang, D. Zhuang, E. Pfender, J. Heberlein, W. Gerberich. in: C.C. Berndt, S. Sampath, (Eds.), Proceedings of the Seventh International Thermal Spray Conference, Boston, MA. ASM International, Materials Park, OH, USA, 1994, p. 587.
[8] L.J. Grant, The Welding Institute, in: I.A. Bucklow, (Ed.), Proceedings of Twelfth International Thermal Spraying Conference, London, UK, paper 111, 1989.
[9] P. Zajchowski, H.B. Crapo, III, J. Therm. Spray Technol. 5 (1996) 457.
[10] H. Liao, Z.Q. Feng, G. Jandin, C. Coddet, Meeting of SF2M West and GFAC on Residual Stresses, St Nazaire, France, 2001, LAMM-St Nazaire, 2001, p. 139.
[11] H.-D. Steffens, K. Nassenstein, J. Therm. Spray Technol. 8 (3) (1999) 454.
[12] T. Watanabe, X. Wang, J. Heberlein, E. Pfender, W. Herwig, in: C.C. Berndt (Ed.), Thermal Spray: Practical Solutions for Engineering Problems, 1996, Cincinnati, ASM International, Materials Park, OH, USA, 1996, p. 577.
[13] N.A. Hussary, J.V.R. Heberlein, J. Therm. Spray Technol. 10 (4) (2001) 604.
[14] G. Jandin, Ph.D. Thesis, Université de Technologie de Belfort-Montbéliard, France, 2001.